

1 **Genome-Wide Detection of Imprinted Differentially Methylated Regions Using**
2 **Nanopore Sequencing**

3 Vahid Akbari^{1,2}, Jean-Michel Garant¹, Kieran O'Neill¹, Pawan Pandoh¹, Richard Moore¹, Marco A.
4 Marra^{1,2}, Martin Hirst^{1,3}, Steven J.M. Jones^{1,2*}.

5 1- Canada's Michael Smith Genome Sciences Centre, British Columbia Cancer Agency, Vancouver,
6 British Columbia, Canada

7 2- Department of Medical Genetics, University of British Columbia, Vancouver, British Columbia,
8 Canada

9 3- Department of Microbiology and Immunology, Michael Smith Laboratories, University of British
10 Columbia, Vancouver, British Columbia, Canada

11 * Author for correspondence: Steven J.M. Jones (sjones@bcgsc.ca)

12 **Abstract**

13 Imprinting is a critical part of normal embryonic development in mammals, controlled by defined parent-
14 of-origin (PofO) differentially methylated regions (DMRs) known as imprinting control regions. As we
15 and others have shown, direct nanopore sequencing of DNA provides a mean to detect allelic methylation
16 and to overcome the drawbacks of methylation array and short-read technologies. Here we leverage
17 publicly-available nanopore sequence data for 12 standard B-lymphocyte cell lines to present the first
18 genome-wide mapping of imprinted intervals in humans using this technology. We were able to phase
19 95% of the human methylome and detect 94% of the well-characterized imprinted DMRs. In addition, we
20 found 28 novel imprinted DMRs (12 germline and 16 somatic), which we confirmed using whole-genome
21 bisulfite sequencing (WGBS) data. Analysis of WGBS data in mouse, rhesus, and chimp suggested that
22 12 of these are conserved. We also detected subtle parental methylation bias spanning several kilobases
23 at seven known imprinted clusters. These results expand the current state of knowledge of imprinting,
24 with potential applications in the clinic. We have also demonstrated that nanopore long reads, can reveal
25 imprinting using only parent-offspring trios, as opposed to the large multi-generational pedigrees that have
26 previously been required.

27 **Introduction**

28 The addition of a methyl group to the 5-carbon of cytidine is the most prevalent and stable epigenetic
29 modification of human DNA (Laurent et al., 2010). DNA methylation is involved in gene regulation and
30 influences a vast array of biological mechanisms, including embryonic development and cell fate, genome
31 imprinting, X-chromosome inactivation, and transposon silencing (Moore et al., 2013; Smith and
32 Meissner, 2013). In mammals, there are two copies or alleles of a gene, one inherited from each parent.
33 Most gene transcripts are expressed from both alleles. However, there is a subset of genes which are
34 expressed from a single allele either randomly such as in X-inactivation, or based upon PofO. The latter
35 is known as imprinting (Chess, 2013; Khamlichi and Feil, 2018).

36 In imprinting, mono-allelic expression of a gene or cluster of genes is controlled by a *cis-acting* imprinting
37 control region (ICR) (Bartolomei and Ferguson-Smith, 2011). The main mechanism by which this occurs
38 is PofO-defined differential methylation at ICRs, also known as imprinted differentially methylated
39 regions (DMRs) (Bartolomei and Ferguson-Smith, 2011; Maupetit-Méhouas et al., 2016). ICRs are
40 classified as germline (or primary) or somatic (or secondary), hereinafter referred to as gDMR and sDMR.
41 Germline ICRs are established during the first wave of methylation reprogramming at germ cell
42 development and escape the second methylation reprogramming after fertilization (Zink et al., 2018).
43 Secondary or somatic ICRs are established *de-novo* after fertilization during somatic development, usually
44 under the control of a nearby primary ICR (Zink et al., 2018). Imprinted clusters of genes may span up to
45 ~4 Mb, by acting through a CCCTC-binding factor (CTCF) binding site or by allelic expression of a long
46 non-coding RNA (Bartolomei and Ferguson-Smith, 2011; da Rocha and Gendrel, 2019). By contrast,
47 individually-imprinted genes are typically regulated by PofO-derived differential methylation at the gene
48 promoter (Bartolomei and Ferguson-Smith, 2011).

49 Imprinting is implicated in various genetic disorders, either from aberrations in imprinting itself, or from
50 deleterious variants affecting the expressed allele at an ICR. Loss of imprinting is also widely observed in
51 human cancers (Goovaerts et al., 2018; Jelinic and Shaw, 2007; Tomizawa and Sasaki, 2012). Thus,
52 accurate mapping and characterization of ICRs in humans is key to the treatment and actionability of
53 genetic disorders, and to personalized oncogenomics.

54 To detect ICRs, accurate assignment of methylation data to paternal and maternal alleles is required.
55 Achieving this with traditional bisulfite sequencing or arrays is challenging. Several studies have used
56 samples with large karyotypic abnormalities, such as uniparental disomies (UPDs), teratomas, and
57 hydatidiform moles, to infer regions of imprinting [14–16]. This approach relies on rare structural variants,
58 but also on the assumption that both normal methylation and the imprinted state remain intact in spite of
59 substantial genomic aberrations. A much larger study by Zink *et al.* leveraged a genotyped, multi-
60 generation pedigree spanning nearly half the population of Iceland (n=150,000), in combination with
61 whole genome oxidative bisulfite sequencing (oxBS-Seq), to phase methylation and infer parent-of-origin
62 (Zink et al., 2018). However, despite being able to phase nearly every SNP in that cohort, they were only
63 able to phase 84% of CpG methylation (CpGs on chromosomes 1-22) in over 200 samples due to the short
64 length of reads. Further, that study was based on a single, genetically-isolated population, which may not
65 be representative of the wider human population. A comprehensive mapping of ICRs using a technology
66 more suited to phasing reads, based on individuals more representative of the human population, could
67 greatly advance our understanding of imprinting, with direct benefits for human health.

68 We have previously shown that nanopore sequencing can detect allelic methylation in a single sample and
69 accurately determine PofO using only trio data. We also developed the software NanoMethPhase for this
70 purpose (Akbari et al., 2021). Here, we applied NanoMethPhase to public nanopore data from a diverse
71 set of 12 lymphoblastoid cell lines (LCLs) from the 1,000 Genomes Project (1KGP) and Genome in a
72 Bottle (GIAB) to investigate genome-wide allele-specific methylation (ASM) and detect novel DMRs

73 (Figure 1A) (De Coster et al., 2019; Shafin et al., 2020; Zook et al., 2019, 2016). Using trio data from
74 1KGP for these cell lines we phased nanopore long reads to their PofO and inferred allelic methylation
75 (Akbari et al., 2021; Auton et al., 2015). Nanopore was able to detect haplotype and methylation status
76 for 26.5 million autosomal CpGs (Chromosomes 1-22), which represents 95% of the autosomal CpGs in
77 the GRCh38 (Kent et al., 2002). We further used public whole-genome bisulfite sequencing (WGBS) data
78 to confirm the presence of the detected DMRs in other tissues and to class the novel DMRs as being
79 germline or somatic. We captured 94% of the well-characterized DMRs (Those reported by at least two
80 studies) and detected 28 novel DMRs (12 germline and 16 somatic). We determined that 43% of these
81 novel DMRs show evidence of conservation in rhesus and chimp. Collectively, our results extend the set
82 of known imprinted intervals in human and demonstrate a major contribution in our ability to characterize
83 imprinting by ASM, brought about by the capabilities of nanopore sequencing.

84 **Results**

85 **Assessing the Effectiveness of Nanopore Methylation Calling and Detection of Known Imprinted** 86 **DMRs**

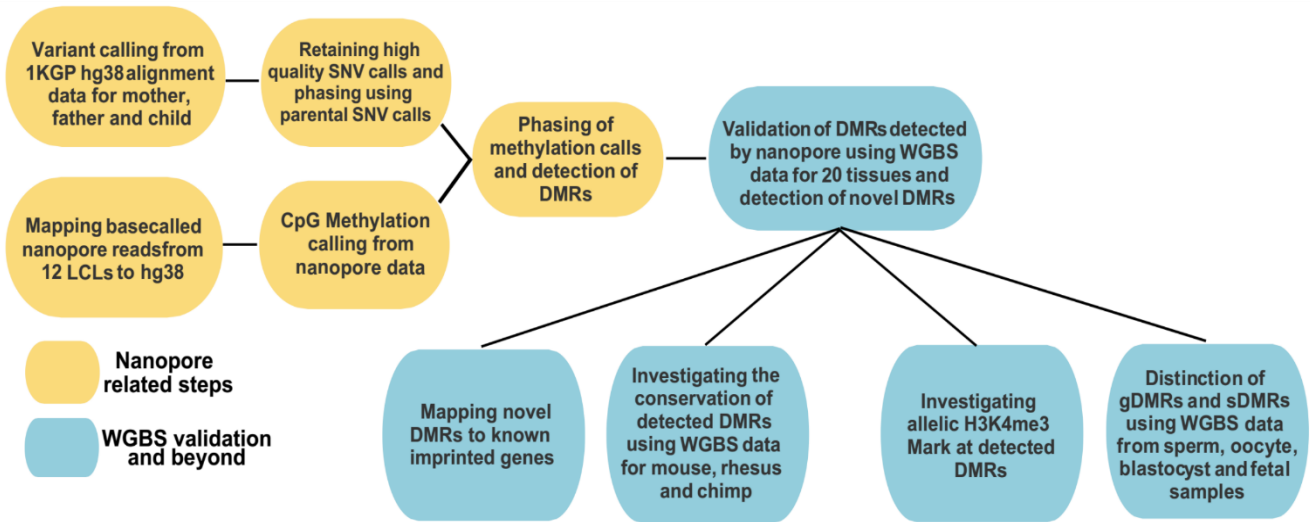
87 We performed correlation analysis among cell lines and NA12878 nanopore-called methylation with
88 WGBS data (ENCFF835NTC) to confirm the reliability of methylation calling (Figure 1B). We observed
89 high correlation across cell lines ($r = 0.75-0.93$), as expected due to their being the same cell type.
90 NA12878 nanopore-called methylation also showed the highest correlation ($r = 0.89$) with NA12878
91 WGBS (Figure 1B), as expected. Additionally, to examine performance on detection of known DMRs,
92 we gathered the list of reported DMRs from previous studies (Court et al., 2014; Hernandez Mora et al.,
93 2018; Joshi et al., 2016; Zink et al., 2018). This included 383 imprinted intervals, of which 68 we assigned
94 as “well-characterized” because they were reported by at least two genome-wide mapping studies or were
95 previously known to be imprinted (Supplementary file1). Subsequently, we haplotyped the methylome in
96 each cell line, performed differential methylation analysis (DMA) between alleles across cell lines. 95%
97 (26.5M) of human autosomal CpGs could be assigned to a haplotype. We detected 172 allelic DMRs (p -
98 value < 0.001 , $|\text{methylation difference}| > 0.25$, and detected in at least 4 cell lines in each haplotype). See
99 supplementary file 2 for more details. Of the 172 detected DMRs, 96 (56%) overlapped with at least one
100 previously reported, while the remaining 76 (44%) were novel. Of the well-characterized DMRs (those
101 detected in at least two previous whole-genome mapping studies or known from prior evidence), 64/68
102 (94%) were detected in our study (Figure 1C, supplementary file2). All DMRs which overlapped with
103 previously-reported DMRs displayed consistent PofO with those studies.

104 We similarly examined the power of nanopore sequencing to detect allelic DMRs within a single sample,
105 by comparing to previous studies (Court et al., 2014; Hernandez Mora et al., 2018; Joshi et al., 2016; Zink
106 et al., 2018). On average, 88% ($M \pm SD = 24.5M \pm 1.7M$) of the human methylome could be assigned to

107 a parental haplotype in each LCL. Of the well-characterized DMRs, ~71% ($M \pm SD = 48 \pm 4.8$) could be
108 detected in a single LCL. An additional 32 DMRs ($SD = 9.7$) reported by only one previous study were
109 detected in each sample (Supplementary figure S1).

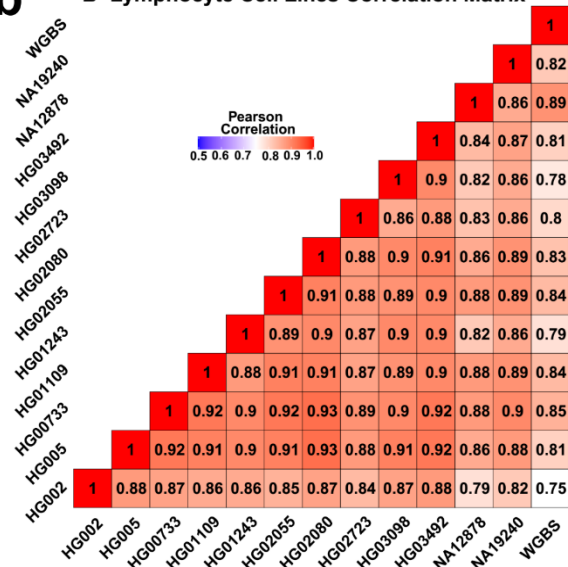
110

a



b

B-Lymphocyte Cell Lines Correlation Matrix



c

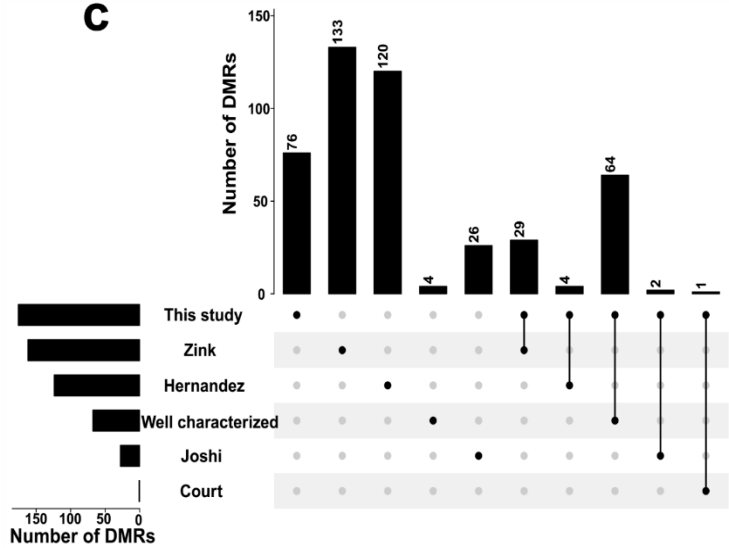


Figure 1: Detection of allelic methylation using nanopore sequencing. a) The flowchart of the study representing all the analysis steps. b) Pearson correlation matrix of the nanopore CpG methylation frequencies for the 12 LCLs and NA12878 whole-genome bisulfite sequencing. c) Upset plot of the number of DMRs detected by us and previous studies and their overlaps.

111 **Confirmation of Novel Imprinted DMRs**

112 As noted above, we detected 76 allelic DMRs that did not overlap with previously-reported ICRs (Court
113 et al., 2014; Hernandez Mora et al., 2018; Joshi et al., 2016; Zink et al., 2018). In order to determine their
114 validity as novel DMRs, we used 24 WGBS datasets from 20 tissue samples within the Roadmap
115 Epigenomics Project (See materials and methods) (Bernstein et al., 2010). We first examined the 96 allelic
116 DMRs which overlapped with the reported DMRs. 79 out of 96 DMRs that overlapped with reported
117 regions showed adjusted p-value < 0.000005 and log2 fold change > 0.15 , while only 5, 6, 7, and 8
118 intervals were detected as significant in the control intervals including 200 randomly selected 1kb bins,
119 CpG islands, 2kb, and 3kb bins, respectively (Figure 2A, Supplementary file 3). Applying this approach
120 to the 76 not previously reported DMRs, the WGBS data supported 28 significant DMRs (Figure 2A and
121 2B, Supplementary file 3). In agreement with previous studies reporting higher number of maternally
122 methylated intervals, 10 of the 28 novel DMRs were paternally methylated and 18 were maternally
123 methylated (Court et al., 2014; Hernandez Mora et al., 2018; Joshi et al., 2016). Overall, 107 out of 172
124 DMRs were validated in tissue WGBS data from which 28 were novel and 79 were reported by the
125 previous studies (Figure 2C, Supplementary file 2) (Court et al., 2014; Hernandez Mora et al., 2018; Joshi
126 et al., 2016; Zink et al., 2018).

127 We also sought to examine the significance of the other 283 previously reported imprinted regions which
128 did not overlap with our detected DMRs. We examined these 283 DMRs in WGBS data and only 139/283
129 DMRs (49%) were significant (adjusted p-value < 0.000005 and log2 fold change > 0.15 . Supplementary
130 file 4). We also mapped these 283 intervals to the DMRs detected in each LCL sample. 81/283 (27%) of
131 them were detected in at least one sample with consistent reported PofO, of which 41 were in common
132 with WGBS analysis (Supplementary file 5).

133

134

135 **Determination of Germline vs Somatic Status of Novel Imprinted DMRs**

136 We performed DMA between oocyte and sperm and overlapped detected DMRs to the 28 novel DMRs.
137 12 of the novel DMRs overlapped with DMRs from oocyte versus sperm (p-value < 0.001. More than
138 40% methylation in oocyte and less than 20% in sperm and vice versa) from which 11 were maternally
139 methylated and 1 was paternally methylated (Figure 3). We then examined the methylation of somatic and
140 germline DMRs in early human embryonic cells and fetal tissues to investigate whether the imprinting of
141 the 12 candidate gDMRs survived the second round of de- and re-methylation and if the other 16 novel
142 sDMRs were established during development. We used blastocyst WGBS data from early cleavage-stage
143 embryos and fetal tissue (Bernstein et al., 2010; Okae et al., 2014). All novel candidate gDMRs showed
144 partial methylation in the blastocyst indicating the gDMRs escaped de-methylation after fertilization
145 (Figure 3). All novel gDMRs and sDMRs displayed partial methylated in fetal tissues indicating survival
146 of gDMRs during somatic development and establishment of sDMRs. Overall, 12 of the novel DMRs
147 detected to be germline while 16 detected as sDMRs (Figure 2C and Figure 3, Supplementary file 6).

148

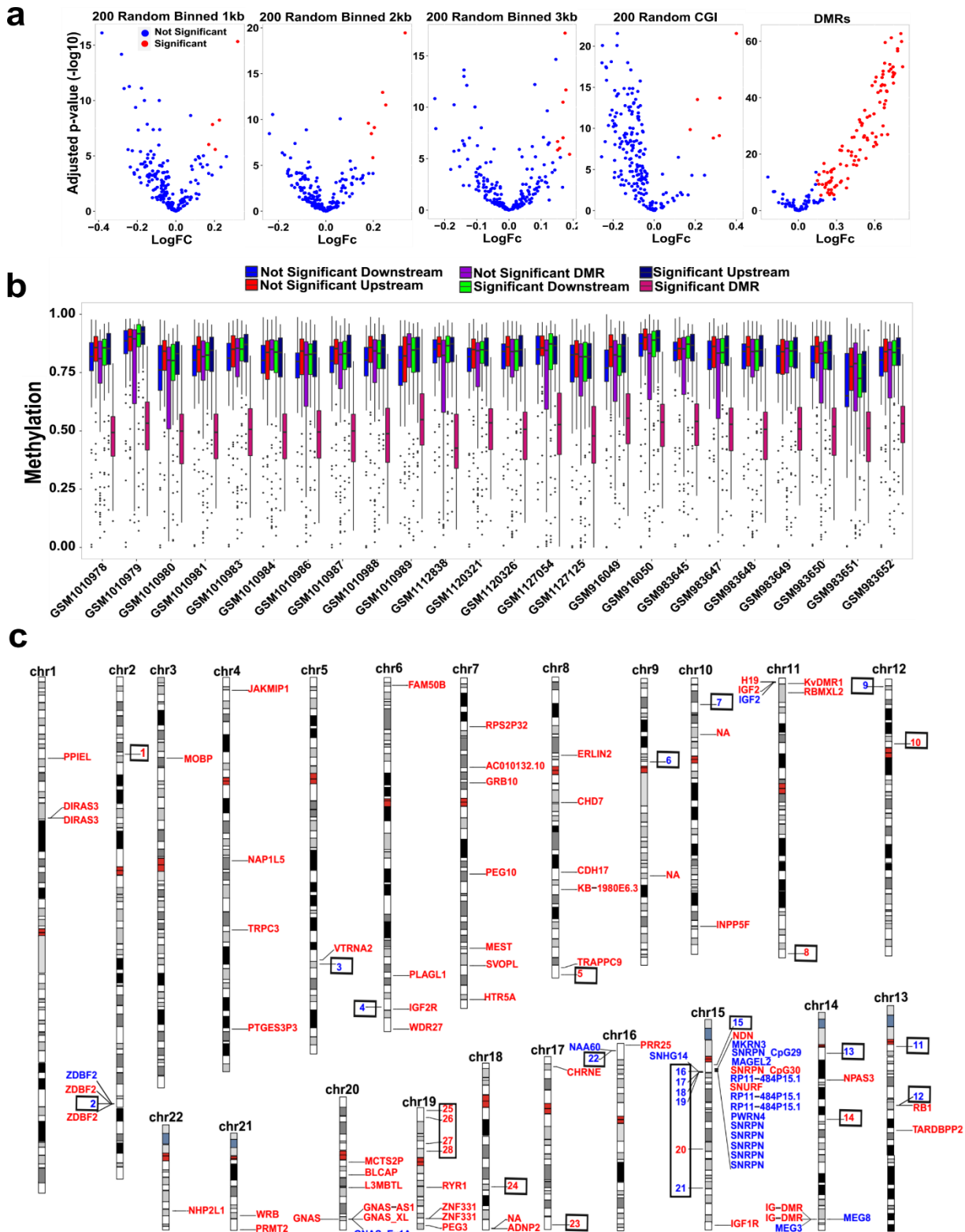
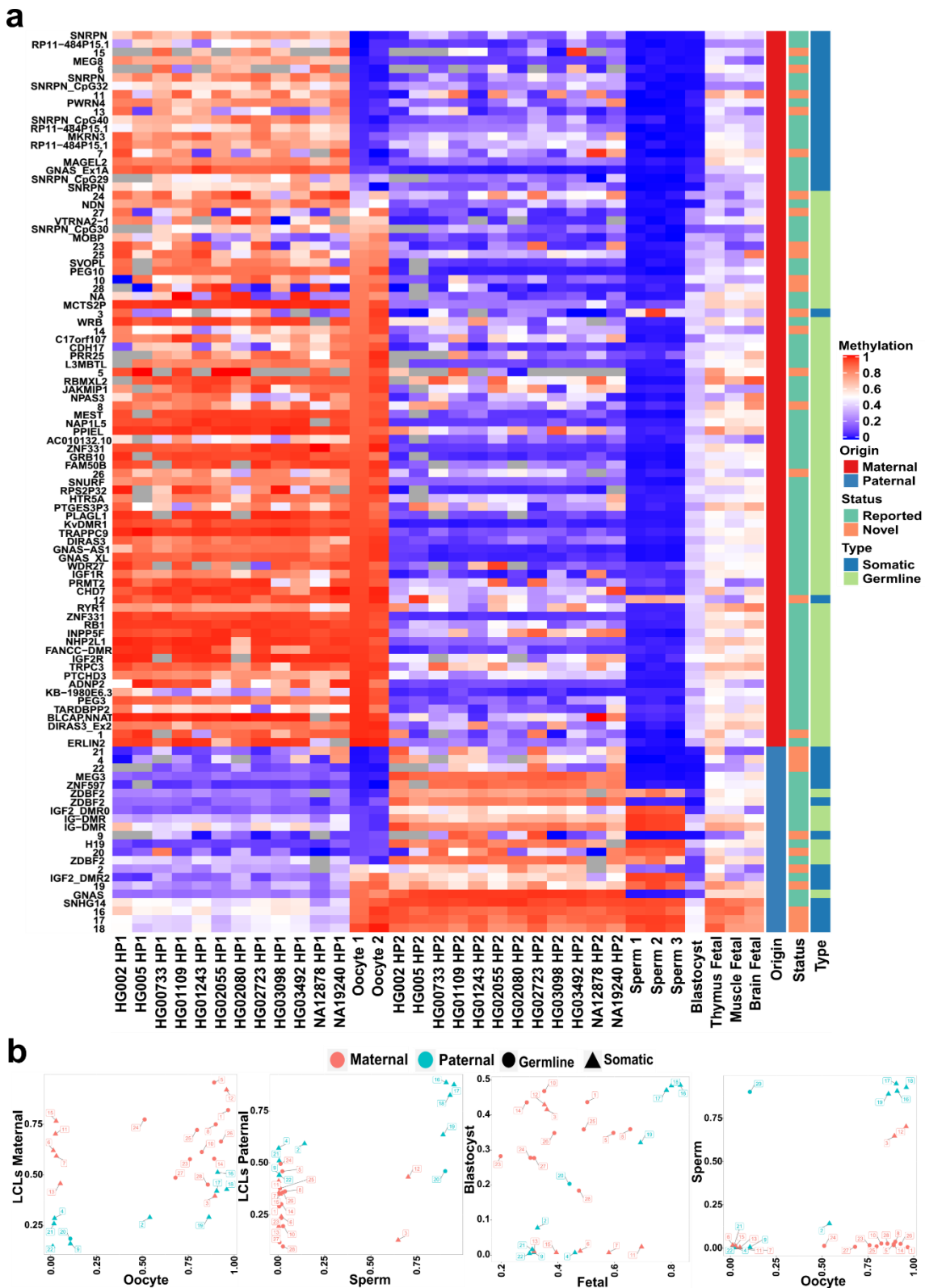


Figure 2: Validation of detected DMRs using WGBS data. a) Limma results for partial methylation (30%-70%) of DMRs detected using nanopore in 20 tissue samples WGBS data along 200 randomly selected CpG islands, 1kb, 2kb, and 3kb intervals as controls. Red dots adjusted p-value < 0.000005 and log₂ fold change > 0.15. b) Box plot showing partial methylation at significant DMRs while not significant DMRs and adjacent regions (down- and upstream to significant and not significant DMRs) are not partially methylated. c) Idiogram of the 107 DMRs which validated by WGBS. On the left on each chromosome are paternally methylated DMRs and on the right are maternally methylated DMRs. Red color represents gDMRs and blue represents sDMRs. Novel DMRs are boxed and numbered.

149



150 **Allelic Histone Methylation of H3K4 is Enriched at Germline DMRs**

151 The H3K4me3 histone mark is protective to DNA methylation. At ICRs, the unmethylated allele is usually
152 enriched for this histone modification (Court et al., 2014; John and Lefebvre, 2011). We used H3K4me3
153 chromatin immunoprecipitation sequencing (ChIP-seq) data for 7 LCLs and their heterozygous single-
154 nucleotide variant (SNV) calls from 1KGP. 81/107 of the detected DMRs could be examined (See material
155 and methods). Of these, 43 reported and 9 novel DMRs showed a significant allelic count in ChIP-seq
156 data (Fisher's combined p-value binomial < 0.01) (Supplementary files 6 and 7). Among the 7 LCLs with
157 ChIP-seq data, only NA12878 and NA19240 were among LCLs with nanopore data and a phased
158 methylome. Therefore, we examined if the allelic H3K4me3 and methylation are in opposite alleles in
159 these cell lines. 23 reported and 5 novel DMRs were significant for allelic H3K4me3 in NA12878 and/or
160 NA19240. 21 reported and 4 novel DMRs showed opposite allelic state between H3K4me3 and
161 methylation (Supplementary file 7).

162 Allelic H3K4me3 mostly overlapped with gDMRs. Overall, 77% of assessable gDMRs and 39% of
163 sDMRs were significant for allelic H3K4me3. This is consistent with previous studies demonstrating the
164 protective role of H3K4me3 against DNA methylation, specifically at germline ICRs in the second round
165 of re-methylation during implantation and somatic development (Chen and Zhang, 2020; Hanna and
166 Kelsey, 2014).

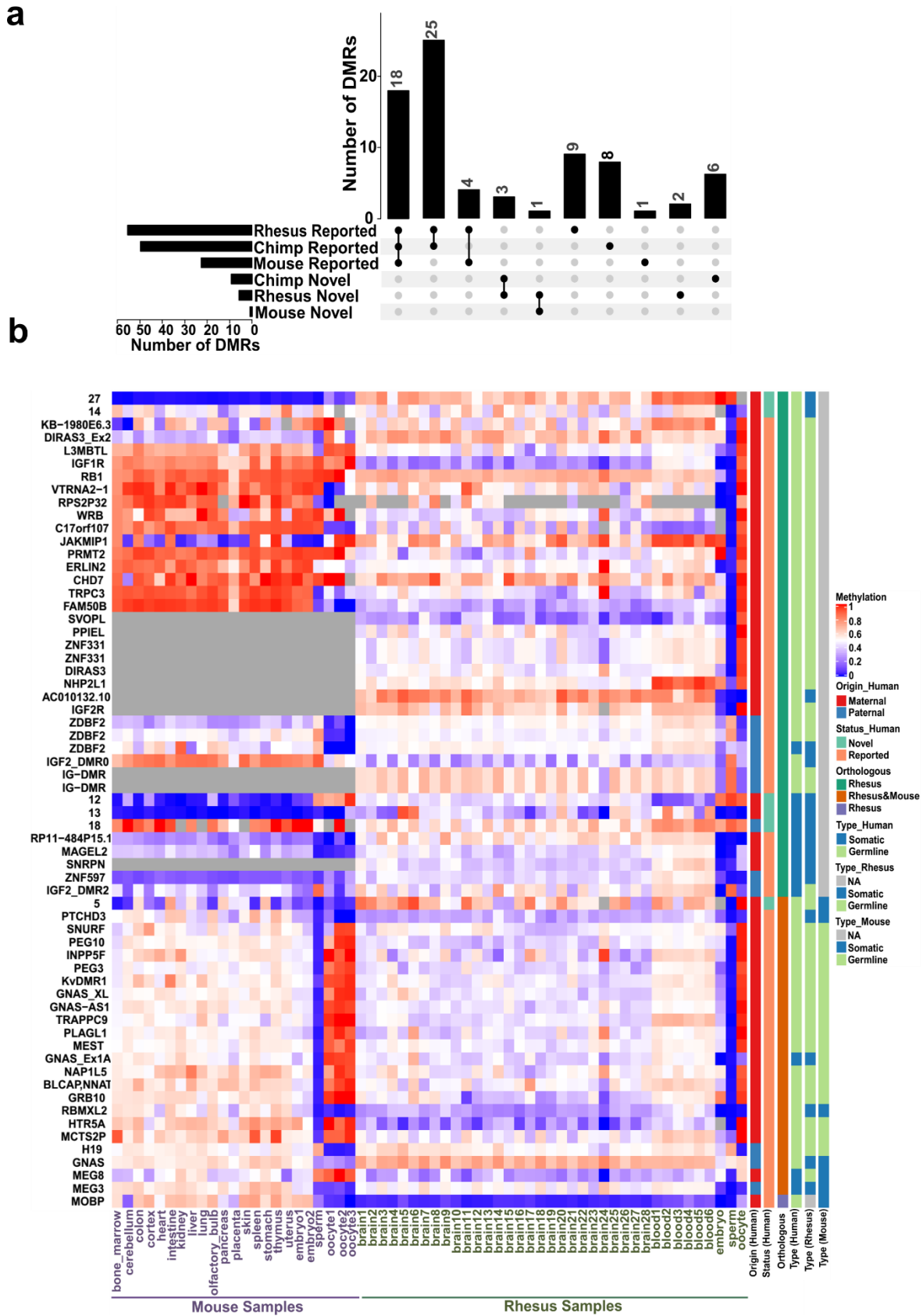
167 **Conservation of Detected Imprinted DMRs across Mammals**

168 To investigate the conservation of detected DMRs and determine if any of the novel DMRs are conserved
169 in mammals we used WGBS data from house mouse (*Mus musculus*), rhesus macaque (*Macaca mulatta*)
170, and chimpanzee (*Pan troglodytes*) (Hon et al., 2013; Tung et al., 2012). We examined whether any of
171 the orthologous regions in these mammals display significant partial methylation (Materials and Methods).
172 Of the 107 DMRs detected by nanopore and validated in WGBS data, 71, 105 and all 107 had orthologs

173 in mouse, rhesus and chimp, respectively. Orthologs of the 77/107 detected DMRs showed significant
174 partial methylated in at least one of the three mammals (Figure 4A, Supplementary file 6). Of these, 65
175 were reported DMRs (56 well-characterized) and 12 novel DMRs. We detected 24 significant orthologous
176 DMRs in mouse. 18 of these were reported to be imprinted by previous studies in mouse (Gigante et al.,
177 2019; Xie et al., 2012). All significant DMRs in mouse, except one, were also significant in rhesus and/or
178 chimp suggesting their existence in their common ancestor. These DMRs mapped to well-known
179 imprinted clusters including *KCNQ1*, *H19*, *GNAS*, *SNURF/SNRPN*, *PLAGL*, *SGCE*, *BLCAP*, *PEG3*,
180 *PEG10*, *PEG13*, *GRB10*, *BLCAP*, *NAP1L5*, *INPP5F*, and *MEG3* where their allelic PofO expression has
181 already been reported in mouse and other mammals (“Geneimprint,” 2021; Morison et al., 2001).

182 Sperm, oocyte and embryo WGBS data for mouse and rhesus were used to investigate if the DMRs that
183 detected as germline or somatic in human are germline or somatic in these mammals and vice versa
184 (Dahlet et al., 2020; Gao et al., 2017; Jung et al., 2017; Saenz-de-Juano et al., 2019). 62 of the human
185 DMRs had significant orthologs in rhesus. Of these, 51 were germline and 11 were somatic in human and
186 in rhesus 45 were germline and 17 were somatic (More than 40% methylation in oocyte and less than 20%
187 in sperm and vice versa. Figure 4B). 24 human DMRs had significant orthologs in mouse. Of these, 21
188 were germline and 3 were somatic in human and in mouse 17 were germline and 7 were somatic (Figure
189 4B). Nine gDMRs in human were somatic in rhesus and/or mouse and three gDMRs from mouse or rhesus
190 were somatic in human. This is consistent with previous studies indicating imprinting is largely conserved
191 in mammals while ICR identity at the germline stage is not completely conserved (Cheong et al., 2015).

192



193 **Novel DMRs within Known Imprinted Gene Domains and Contiguous Blocks of** 194 **Parental Methylation Bias**

195 We gathered the list of 259 imprinted genes from previous studies (Supplementary file 8) (Babak et al.,
196 2015; Baran et al., 2015; “Geneimprint,” 2021; Jadhav et al., 2019; Morison et al., 2001; Zink et al.,
197 2018). 14 novel DMRs (6 germline and 8 somatic) mapped close (<1.03Mb) to imprinted genes
198 (Supplementary file 6 and 9).

199 Of the 8 sDMRs close imprinted genes, only one mapped to a CpG island, and that was a small
200 (<300bp) CpG island ~13 Kb downstream of the maternally expressed *NAA60* gene (Supplementary
201 figure S2). Four novel sDMRs (All paternally methylated) mapped in the Prader-Willi syndrome and
202 Angelman syndrome (PWS/AS) cluster. Previous studies reported continuous subtle paternal
203 methylation bias at the PWS/AS cluster (Hernandez Mora et al., 2018; Joshi et al., 2016; Zink et al.,
204 2018). Consistent with previous studies, the four novel sDMRs at this cluster were large (>5Kb) and
205 seemed to constitute near-continuous paternal methylation spanning a ~200kb region. This included the
206 *SNORD116* cluster genes and several other genes such as *PWARI* and *6*, *PWARSN* and *IPW*
207 (Supplementary figure S3). This paternally methylated somatic block is downstream of the maternally
208 methylated germline *SNURF/SNRPN* ICR, which is associated with PWS and shows evidence of
209 conservation in chimp, rhesus, and mouse. Moreover, the allele-specific expression (ASE) track from
210 Zink *et al.* displayed strong paternal expression across this ~200kb region (Zink et al., 2018). Another
211 three novel sDMRs mapped close *RBI/LPAR6*, *IGF2R* (Supplementary figures S4 and S5) and *GPR1-*
212 *AS/ZDBF2*. The novel sDMR at *GPR1-AS/ZDBF2* were close to 2 known paternal gDMRs. Moreover,
213 LCLs PofO methylation track at the *ZDBF2* gene body showed continuous subtle paternal bias.
214 Together, these suggest a ~65kb paternally methylated block interrupted by unmethylated CpG island at
215 *ZDBF2* promoter (Supplementary figure S6). In addition to blocks with novel DMRs, we sought to
216 detect continuous block of parental methylation bias at other regions. We detected 5 other contiguous

217 blocks of imprinting at *ZNF331*, *KCNQ1OT1*, *GNAS*, *L3MBTL1* and *ZNF597/NAA60*, ranging from 35-
218 58Kb in size (Supplementary figures S7-11).

219 All the six gDMRs within imprinted gene domains were maternally methylated and they all mapped to
220 CpG islands except a DMR mapped in the *AC024940.1 (OVOS2)* (Supplementary figures S12-16,
221 Figure 5). Five of them mapped to known imprinted genes without previously reported DMR or a DMR
222 with a much greater distance from the gene compared to our DMRs including *AC024940.1*, *ZNF714*,
223 *DDAI1*, *ADAMTSL5*, and *NAPRT* (Court et al., 2014; Hernandez Mora et al., 2018; Joshi et al., 2016;
224 Zink et al., 2018). A novel gDMR mapped to the promoter of *ZNF714* which is reported to be
225 paternally expressed (Jadhav et al., 2019; Zink et al., 2018). Thus suggesting this DMR could be the
226 potential ICR and directly suppress maternal allele by blocking its promoter (Figure 5). *AC024940.1*
227 reported to be paternally expressed (Zink et al., 2018). A novel germline maternal DMR mapped near
228 the end of the *AC024940.1* gene (encompassing the intron 38 to the start of exon 40) adjacent to a CTCF
229 binding site (Supplementary figure S12). *DDAI1* and *ADAMTSL5* have been previously reported to be
230 maternally expressed and *NAPRT* has an isoform dependent expression origin (Babak et al., 2015; Zink
231 et al., 2018). A gDMR mapped to the end and downstream of *DDAI1* gene (Supplementary figure S13).
232 For *ADAMTSL5* and *NAPRT*, gDMRs mapped close to these genes (<150Kb) (Supplementary figures
233 S14 and S15).

234

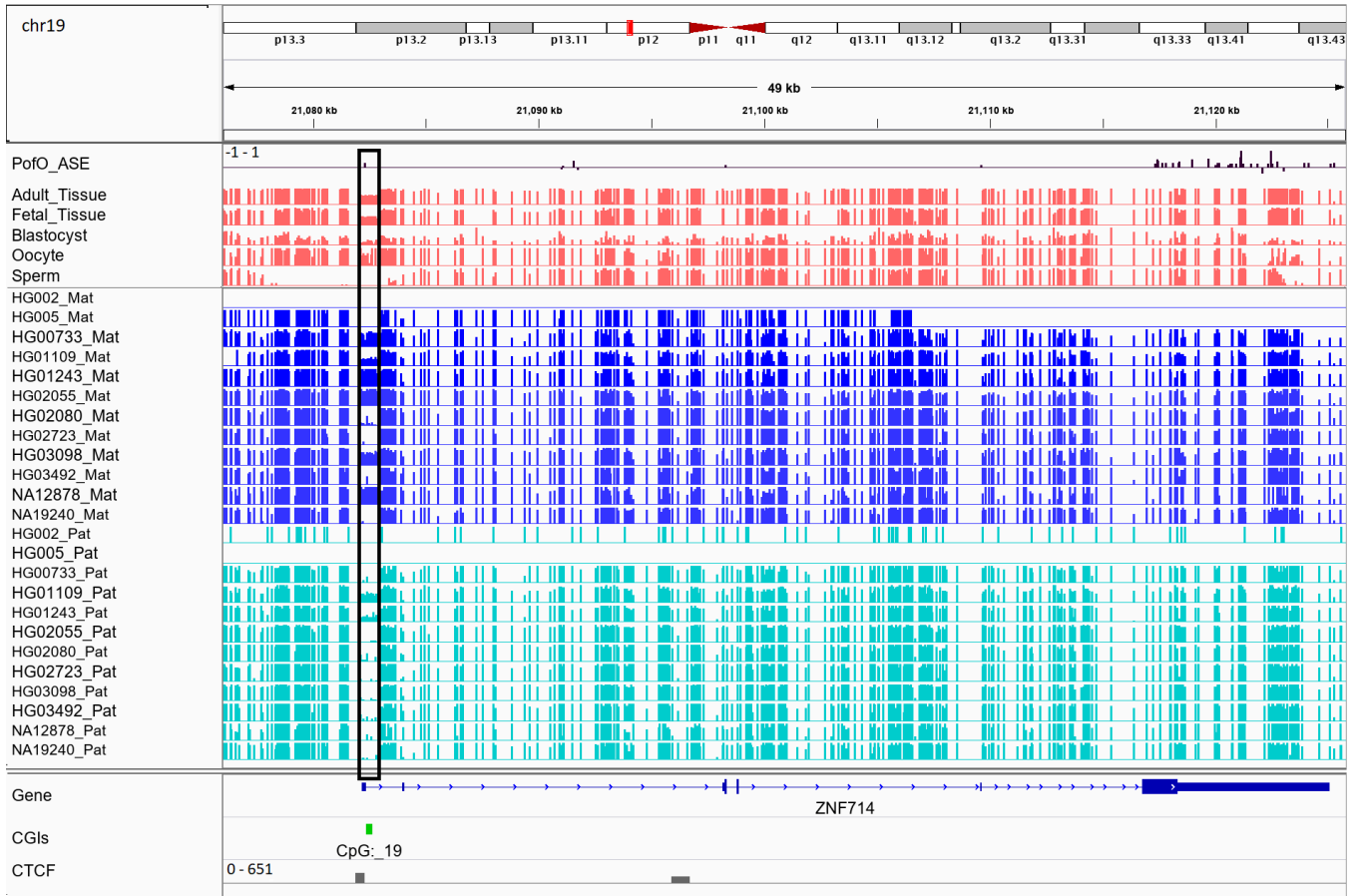


Figure 5: IGV screenshot of the novel maternally methylated germline DMR at the promoter of the paternally expressed ZNF714 gene. Black box region represents the DMR. PofO_ASE represents allele specific expression track from Zink *et al.* without any filtering for *P* value and positive vertical bars (upward) represents more paternal expression and negative bars (downward) maternal expression. The range for all methylation tracks is 0-1.

235 **Discussion**

236 Here we described the first genome-wide map of human allele-specific methylation using nanopore
237 sequencing. Leveraging long reads and parental SNVs allowed us to phase methylation for ~26.5 million
238 autosomal CpGs representing 95% of the CpGs in the human autosomal genome (GRCh38) across 12
239 LCLs (De Coster et al., 2019; Kent et al., 2002; Shafin et al., 2020; Zook et al., 2016). This represents a
240 much higher resolution than previous studies aimed to capture allelic methylation (Court et al., 2014;
241 Hernandez Mora et al., 2018; Joshi et al., 2016; Zink et al., 2018). For example, Zink *et al.* determined
242 the PofO of almost all genotypes using nearly half the population of Iceland (n=150,000) and used over
243 200 whole-genome OxBS-seq samples to detect imprinting (Zink et al., 2018). They could define PofO
244 methylation for ~23.5 million autosomal CpGs (84%). We noticed three of our novel DMRs did not have
245 any CpG representation from Zink *et al.* Moreover, in a further three other novel DMRs, fewer than 60%
246 of the CpGs were captured in Zink *et al.* (Supplementary file 6). EPIC methylation arrays detect over 850k
247 CpGs and covers almost all CpGs detectable by 450k and 27k methylation arrays. Seven of our novel
248 DMRs did not have any CpGs covered by the EPIC array and 9 other novel DMRs had only 1 or 2 probes
249 on this platform (Supplementary file 6). This highlights the breadth of nanopore sequencing for the
250 purposes of ICR calling.

251 Even though we detected methylation for all the CpGs in the human genome (GRCh38), we were not able
252 to phase 5% of the human methylome (Kent et al., 2002). To phase nanopore reads, we used SNVs
253 detected from short-reads data in the 1KGP (Auton et al., 2015). Short-reads are challenging to map to
254 complex repetitive regions which results in lack of SNVs and subsequent inability to phase reads in these
255 regions. 75% of the unphased CpGs mapped to the ENCODE blacklist (Amemiya et al., 2019). We
256 previously demonstrated that using SNVs detected from nanopore to phase reads results in reliable
257 methylation phasing and detection of a few more reported DMRs (Akbari et al., 2021). Improvement in

258 basecalling and variant calling from nanopore reads could enable the phasing of a complete genome-wide
259 methylome using nanopore detected SNVs.

260 Using nanopore sequencing we could capture 94% of the well-characterized DMRs and 35 of the DMRs
261 reported by only one study (Court et al., 2014; Hernandez Mora et al., 2018; Joshi et al., 2016; Zink et al.,
262 2018). However, we were unable to detect a further 283 DMRs, mostly reported by one previous study
263 (Court et al., 2014; Hernandez Mora et al., 2018; Joshi et al., 2016; Zink et al., 2018). In further analyses,
264 180 of these DMRs were detected in at least one nanopore-sequenced LCL sample and/or validated in the
265 Roadmap multi-tissue WGBS data we used (Supplementary files 4 and 5). We should note that nanopore
266 data comes from a small number of B-lymphocyte cell-line samples, yet considerably diverse in ethnicity.
267 Imprinted DMRs can be tissue-specific and polymorphic across individuals, which may explain this
268 discrepancy (Court et al., 2014; Hernandez Mora et al., 2018; Joshi et al., 2016; Romanelli et al., 2014;
269 Silver et al., 2015; Zink et al., 2018). Characterization of imprinted DMRs across a wider range of tissues
270 and populations represents a clear path forward for the field. The ability of nanopore sequencing to
271 characterize imprinting using only parent-offspring trios represents a relatively low-cost avenue by which
272 this might be achieved.

273 We detected 107 DMRs using nanopore which were further confirmed in multi-tissue WGBS data. Twelve
274 of these were novel gDMRs and sixteen were novel sDMRs not reported in previous studies (Court et al.,
275 2014; Hernandez Mora et al., 2018; Joshi et al., 2016; Zink et al., 2018). These novel DMRs were
276 supported by several lines of evidence in our analyses. 1) They displayed significant PofO methylation
277 bias in nanopore LCLs. 2) They were significantly partially methylated in WGBS data from 20 human
278 tissues. 3) gDMRs demonstrated escape from the second de-methylation step. 4) They were partially
279 methylated in three fetal tissue samples. 5) 43% of those for which H3K4me3 ChIP-seq data could be
280 phased showed significant allelic H3K4me3. 6) 43% showed evidence of conservation in at least one of
281 the three mammals including chimp, rhesus, and mouse. 7) 71% mapped to at least one regulatory region

282 including CpG island, CTCF binding site and enhancer. These novel DMRs represent a substantial and
283 well-validated expansion of known regions of imprinting, which may aid future research and diagnosis in
284 the fields of genetic medicine and oncology.

285 Of the 107 DMRs, 20 mapped to the PWS/AS cluster. Previous studies demonstrated two paradigms of
286 imprinting at this cluster, either PofO methylation confined to particular regulatory regions such as CpG
287 islands or subtle paternal bias across this cluster with spikes of maternal methylation (Court et al., 2014;
288 Joshi et al., 2016; Sharp et al., 2010; Zink et al., 2018). Although we did not observe paternal methylation
289 bias across the whole PWS/AS cluster, we did detect a paternal methylation block spanning ~200Kb,
290 immediately downstream of the known maternally methylated PWS *SNURF/SNRPN* ICR. This block
291 encompasses the *SNORD116* cluster and other adjacent genes with strong paternal expression
292 (Supplementary figure S3). Probes with paternal methylation bias at the *SNORD116* cluster have been
293 reported which span about 95Kb region and paternal deletion of this cluster results in PWS phenotypes
294 (Hernandez Mora et al., 2018; Joshi et al., 2016; Matsubara et al., 2019). Slight hypomethylation of
295 *SNORD116* cluster in cases with PWS phenotype and hypermethylation in the cases with AS phenotype
296 have been reported (Matsubara et al., 2019). Our analysis extends and more clearly delineates this
297 paternally biased block.

298 Beyond the PWS/AS cluster, we detected another six blocks of allelic methylation bias (Supplementary
299 figure S6-S11). All of the blocks represented several common features. 1) They were detected in imprinted
300 genes that appeared in cluster. 2) All of them were accompanied by a strong PofO expression bias from
301 the subtle hypermethylated allele. 3) There was at least one well-characterized and conserved gDMR in
302 each block (except *ZNF597/NAA60* block with a conserved sDMR). 4) The well-characterized DMRs in
303 these blocks displayed significant allelic H3K4me3 (except DMR in *L3MBTL1* block which could not be
304 examined due to the lack of SNV). 5) Well-characterized DMRs in these blocks overlapped to the
305 promoter of genes with subtle PofO methylation bias at the gene body and DMR itself displayed opposite

306 PofO methylation (except for *ZDBF2/GPR1-AS* block that DMR did not map to the promoter and had
307 the same PofO with the gene body). This represents a novel facet of imprinting biology. To explain this,
308 we can consider that CpG methylation at gene bodies is positively (but weakly) correlated with gene
309 expression (Ball et al., 2009; Yang et al., 2014). Within these blocks, we saw parental methylation bias at
310 the parentally expressed or active allele. This may suggest that subtle parental methylation is linked to
311 parental ASE. However, ASE is observed in many other imprinted genes whose gene bodies do not show
312 parental methylation bias. One possible explanation could be that the subtle parental methylation bias is
313 used by cells to express important genes (genes which can regulate other genes in the cluster or have
314 regulatory roles) in an imprinted cluster with higher fidelity through its gene body methylation on active
315 allele. For example, at the *KCNQ1OT1* and *GNAS* clusters the methylation blocks overlap *KCNQ1OT1*
316 and *GNAS-AS1* genes both of which encode antisense RNA transcripts that regulate other genes in the
317 imprinted cluster (Chiesa et al., 2012; Turan and Bastepe, 2013). However, further studies are needed to
318 reveal the mechanism producing these contiguous slight parental methylation bias blocks and their
319 functional role.

320 Orthologous regions of ~72% of the detected DMRs were demonstrated significant partial methylation in
321 at least one of the chimp, rhesus, and mouse. There were a considerably higher number of orthologous
322 sites and significant orthologous DMRs in chimp and rhesus in agreement with more similarities and less
323 distance to these primates compare to mouse in the human evolution. Orthologs of the 12 novel DMRs
324 were mostly displayed significant partial methylation in rhesus and/or chimp while the other 16 novel
325 DMRs were not significant in any of the examined mammals (Figure 4). This suggests that the novel
326 DMRs (except one which had significant orthologous in mouse) are established after divergence of
327 primates' common ancestor from mouse and majority of them established after the divergence of human
328 common ancestor from chimp. Court *et al.* detected 14 novel DMRs, at the time of their study, and did
329 not detect any imprinted orthologs of their novel DMRs in mouse (Court et al., 2014). All 14 also

330 overlapped with our detected DMRs and six of them had orthologous regions in mm10 using the UCSC
331 liftover file (Kent et al., 2002). Two of the orthologs displayed partial methylation in mouse, one in *Rian*
332 gene which did not examined in Court *et al.* and the other in *Htr5a* gene which reported not to be conserved
333 in mouse by Court *et al.* (Court et al., 2014). When looking into their analysis, it seems that they examined
334 different orthologous region (Supplementary figure S19). For *Htr5a*, they examined the CpG island
335 (CpG:_102) ~50 kb away from the gene while we examined the region spanning the first or second exon
336 (two transcripts) of *Htr5a* which was partially methylated while CpG:_102 was also unmethylated in our
337 study.

338 Using reported imprinted genes, 50% of the novel DMRs mapped close to known imprinted genes (Babak
339 et al., 2015; Baran et al., 2015; “Geneimprint,” 2021; Jadhav et al., 2019; Morison et al., 2001; Zink et al.,
340 2018). Five of our novel gDMRs could be potential ICRs for reported imprinted genes without reported
341 ICR. Specifically, maternal methylation of CpG island overlapping promoter of *ZNF714* as it can directly
342 repress maternal allele and results in the reported paternal expression (Figure 5) (Jadhav et al., 2019; Zink
343 et al., 2018). *ZNF714* is a member of the zinc finger family proteins which have several imprinted genes
344 with developmental roles (Babak et al., 2015; Baran et al., 2015; Camargo et al., 2012; Jadhav et al., 2019;
345 Zink et al., 2018). *ZNF714* has been reported to be associated with non-syndromic cleft lip (Camargo et
346 al., 2012). Thus, this new imprinted DMR could be of potential clinical value. In contrast to imprinting
347 which is established in the germline and usually consistent across tissues, allelic expression is only present
348 if the imprinted gene is expressed in the tissue. Moreover, studies have used short read sequencing to
349 detect ASE which is confounded with several limitations (Aird et al., 2011; Steijger et al., 2013).
350 Therefore, a comprehensive ASE analysis using long-read technologies capturing various tissues might
351 explain ASE around the novel DMRs without evidence of a close imprinted gene. Paternal expression bias
352 of *PTCHD3* and maternal expression bias for *FANCC* are detected in Zink *et al.* while they could not
353 detect any associated DMR (Zink et al., 2018). Hernandez *et al.* detected 3 and 1 maternally methylated

354 probes at the promoter of *PTCHD3* and intron one of *FANCC*, respectively, but were not able to examine
355 the parental expression (Hernandez Mora et al., 2018). We also detected two maternally methylated
356 gDMRs overlapping the promoter of *PCTHD3* and intron one of *FANCC* (Supplementary figures S17 and
357 S18). There were no phased CpG for these DMRs in Zink *et al.* study (Supplementary file 6). Orthologous
358 regions for the *PTCHD3* DMR were also detected to be partially methylated in all three mammals but the
359 *FANCC* DMR was only partially methylated in chimp. These gDMRs could potentially explain the
360 missing ICR for ASE of these genes. The gDMR at the *PTCHD3* promoter can directly suppress maternal
361 allele. *FANCC* gDMR overlaps to a CpG island and CTCF binding site. CTCF is a methylation sensitive
362 DNA-binding protein and CpG methylation can inhibit CTCF binding (Hashimoto et al., 2017; Renda et
363 al., 2007). Moreover, CTCF binding to the first intron of major immediate-early gene of the human
364 cytomegalovirus (HCMV) in HCMV-infected cells resulted in repression of this gene (Puerta et al., 2014).
365 Therefore, the maternally methylated DMR in intron 1 of maternally expressed *FANCC* suggests a
366 mechanism through which paternal allele is suppressed by CTCF binding at DMR while DNA methylation
367 inhibits CTCF binding at maternal allele.

368 Overall, our study represents a near-complete genome-wide map of human allele-specific methylation by
369 leveraging long-read nanopore technology. This allowed us to expand the set of reported imprinted DMRs
370 using just 12 LCLs with parental SNPs and explain novel DMRs as potential ICRs for several imprinted
371 genes with unknown ICR. 43% of the novel DMRs demonstrated partial methylation in other mammals
372 suggesting their conservation. We detected seven large PofO bias methylation blocks spanning multiple
373 kilobasesd and displaying several common features. We have suggested two avenues of further
374 investigation: 1) Looking for tissue and individual polymorphism in imprinting, and 2) determining the
375 mechanism and function of the subtle parental bias blocks. We have also shown that nanopore sequencing
376 is a cheap and easy way to call ICRs and can open the way to answering those questions in future. This
377 study provides a blueprint for further surveys using nanopore sequence data and demonstrates the potential

378 of this approach to study personalized allelic methylation in disease such as cancer with wide spread allelic
379 methylation aberrations.

380 **Materials and Methods**

381 **Nanopore Sequencing Data and Detection of Allele-Specific Methylation**

382 We used publicly available nanopore sequencing data for 12 LCLs including HG002, HG005, HG00733,
383 HG01109, HG01243, HG02055, HG02080, HG02723, HG03098, HG03492, NA12878, and NA19240
384 (ERR3219853 & ERR3219854) (De Coster et al., 2019; Shafin et al., 2020; Zook et al., 2016). All cell
385 lines had trio information available from 1KGP or GIAB (Auton et al., 2015; Zook et al., 2019). Raw
386 nanopore fast5 files along with basecalled fastq files for 12 LCLs were obtained and basecalled reads
387 mapped to GRCh38 using Minimap2 with the setting *minimap2 -ax map-ont* (Kent et al., 2002; Li, 2018).
388 Subsequently, CpG methylations were called using nanopolish with default parameters (Simpson et al.,
389 2017). Methylation calls for each sample preprocessed using NanoMethPhase *methyl_call_processor*
390 module for downstream analysis (Akbari et al., 2021). To detect allelic methylation we first called variants
391 using Strelka2 and default parameters from alignment files of each LCL and its parents obtained from
392 1KGP GRCh38 (Auton et al., 2015; Kim et al., 2018). For HG002 and HG003 variant call data were
393 obtained from GIAB (Zook et al., 2019). For each LCL a mock phased vcf file with defined parent of
394 origin of each high-quality heterozygous SNV was created using an in-house bash script
395 (<https://github.com/vahidAK/NanoMethPhase/tree/master/scripts>: Trio_To_PhaseVCF_4FemaleChild.sh
396 & Trio_To_PhaseVCF_4MaleChild.sh). Subsequently, we detected haplotype methylome in each sample
397 using NanoMethPhase with the setting *nanomethphase phase -mbq 0*. Finally, DMRs between haplotypes
398 were called using NanoMethPhase *dma* module. To avoid the confounding effects of X-inactivation, and
399 because previous studies demonstrated no evidence of imprinting at sex chromosomes, we only examined
400 autosomal chromosomes (Court et al., 2014; Joshi et al., 2016; Zink et al., 2018).

401 **WGBS Data and Detection of Novel DMRs**

402 To validate allelic methylation in other tissues and also detect potential novel ICRs we used 24 public
403 WGBS (GSM1010978, GSM1010979, GSM1010980, GSM1010981, GSM1010983, GSM1010984,
404 GSM1010986, GSM1010987, GSM1010988, GSM1010989, GSM1112838, GSM1120321,
405 GSM1120326, GSM1127054, GSM1127125, GSM916049, GSM916050, GSM983645, GSM983647,
406 GSM983648, GSM983649, GSM983650, GSM983651, GSM983652) for 20 tissue samples from
407 Epigenomics Roadmap including adipose, adrenal gland, liver, aorta, brain hippocampus, breast luminal
408 epithelial, breast myoepithelial, esophagus, gastric, left ventricle, lung, ovary, pancreas, psoas muscle,
409 right atrium, right ventricle, sigmoid colon, small intestine, spleen, and thymus (Bernstein et al., 2010).
410 Wig files which include fractional methylation data were obtained and converted to bed format using
411 UCSC tools and lifted over to hg38 coordinates using CrossMap and UCSC lift over chain file (Kent et
412 al., 2002; Zhao et al., 2014). All, bed format files were then merged to keep CpGs that are common in at
413 least 10 samples. At imprinting control regions only one allele is methylated and we expect to observe
414 partial methylation (~50%) at such regions. However, the adjacent sites which are not imprinted display
415 ~0% or ~100% methylation. Therefore, we used a comparison between detected DMRs with their adjacent
416 sites in WGBS data. For each DMR we determined the number of CpG sites with methylation rates
417 between 30-70% (partial methylation) and normalized it by dividing the numbers to all CpGs in the
418 interval. We also determined this ratio for the adjacent sites (≥ 20 kb away and not been reported as
419 imprinted gene or ICR). We then used limma's linear model to perform statistical analysis of the ratios at
420 each DMR and adjacent sites (Codes are available on
421 <https://github.com/vahidAK/NanoMethPhase/tree/master/scripts>:
422 `PartialCpGMethylationAtDMRandAdjacent.py` and
423 `ComparePartialMethylationAtDMRsToAdjacentUsingLimma.R`). As controls and because ICRs are
424 usually overlapped with CpG islands, we examined 200 randomly selected CpG islands and 200 randomly
425 selected 1kb, 2kb, and 3kb intervals with more than 15 CpGs.

426 **Detection of Germline and Somatic DMRs**

427 If a DMR is germline, it is established during germ cell development and survived the pre-implantation
428 methylation reprogramming. Therefore, gDMRs will overlap with DMR detected from oocyte vs sperm
429 with consistent methylation direction, i.e. maternally methylated DMRs display high methylation in
430 oocyte and very low or no methylation in sperm and vice versa. Moreover, gDMRs need to display partial
431 methylation after fertilization and early development.

432 In order to discriminate gDMRs from somatic, we used public WGBS data for sperm, oocyte, blastocyst,
433 and fetal tissues (GSM1172595 thymus, GSM1172596 muscle, GSM941747 brain) (Bernstein et al.,
434 2010; Okae et al., 2014). Read counts for methylated and unmethylated CpG sites were obtained for sperm
435 and oocyte samples and DMA was performed using NanoMethPhase *dma* module. To detect potential
436 candidate gDMRs, we overlapped detected DMRs from oocyte vs sperm DMA to detected imprinted
437 DMRs from nanopore. We further used blastocyst and fetal tissues to investigate if potential gDMRs
438 escaped the second round of methylation reprogramming and if sDMRs are established during somatic
439 development.

440 **Allelic H3K4me3 Analysis**

441 H3K4me3 ChIP-seq fastq files were obtained for NA12878, NA12891, NA12892, NA19238, NA19239,
442 NA19240, and NA18507 and aligned to the GRCh38 reference genome using bwa-mem default setting
443 (Adoue et al., 2014; Kent et al., 2002; Li and Durbin, 2009). SNVs were called for these samples from
444 1KGP GRCh38 alignment files using strelka2 (Auton et al., 2015; Kim et al., 2018). We then counted the
445 number of reads with minimum mapping quality of 20 and base quality of 10 at each heterozygous SNV
446 and kept those with more than 5 mapped reads for binomial test. The reference allelic counts and total
447 counts at each heterozygous SNV (or maternal allelic counts and total counts in case for trios) were used

448 to detect significant allelic bias using a two-sided binomial test under the default probability of $P = 0.5$ in
449 python SciPy package (Virtanen et al., 2020).

450 **Mammalian Conservation of DMRs**

451 To test whether any of the detected novel DMRs are conserved in other mammals we used WGBS data
452 for mouse (GSE42836), Macaque (GSE34128 and GSE151768), and Chimp (GSE151768) to examine
453 partial methylation in orthologous intervals (Hon et al., 2013; Tung et al., 2012). Mouse, Macaque, and
454 Chimp coordinates lifted over to mm10, RheMac8, and PanTro5 coordinates using CrossMap and
455 appropriate liftover file from UCSC, if they were not already in this coordinates. The list of detected
456 human DMRs were also converted to the orthologous regions for each mammal using CrossMap and the
457 appropriate UCSC liftover file (Kent et al., 2002; Zhao et al., 2014). Since many coordinates in human
458 splinted to several orthologous in other mammals, we merged orthologous intervals which were ≤ 200 bp
459 apart. Finally, we used our approach explained in aforementioned section (WGBS Data and Detection of
460 Novel DMRs) to detect ortologs with significant partial methylation.

461 To examine the somatic and germline orthologous DMRs, we used WGBS data from mouse embryo
462 (GSM3752614, GSM4558210) , sperm (GSE79226) , oocyte (GSM3681773, GSM3681774,
463 GSM3681775) and Rhesus embryo (GSM1466814), sperm (GSM1466810), and oocyte samples
464 (GSM1466811) (Dahlet et al., 2020; Gao et al., 2017; Jung et al., 2017; Saenz-de-Juano et al., 2019).

465 **Acknowledgements:** SJMJ and MM acknowledge funding from the Canada Research Chairs program
466 and the Canadian Foundation for Innovation. VA acknowledge funding from the University of British
467 Columbia Four Year Doctoral Fellowship.

468 **Competing interests:** The authors declare that there is no competing interests.

469 References

- 470 Adoue V, Schiavi A, Light N, Almlöf JC, Lundmark P, Ge B, Kwan T, Caron M, Rönnblom L, Wang C,
471 Chen S-H, Goodall AH, Cambien F, Deloukas P, Ouwehand WH, Syvänen A-C, Pastinen T. 2014.
472 Allelic expression mapping across cellular lineages to establish impact of non-coding SNPs. *Mol*
473 *Syst Biol* **10**:754.
- 474 Aird D, Ross MG, Chen W-S, Danielsson M, Fennell T, Russ C, Jaffe DB, Nusbaum C, Gnirke A. 2011.
475 Analyzing and minimizing PCR amplification bias in Illumina sequencing libraries. *Genome Biol*
476 **12**:1–14.
- 477 Akbari V, Garant J-M, O’Neill K, Pandoh P, Moore R, Marra MA, Hirst M, Jones SJM. 2021.
478 Megabase-scale methylation phasing using nanopore long reads and NanoMethPhase. *Genome Biol*
479 **22**:68.
- 480 Amemiya HM, Kundaje A, Boyle AP. 2019. The ENCODE Blacklist: Identification of Problematic
481 Regions of the Genome. *Sci Rep* **9**:9354.
- 482 Auton A, Abecasis GR, Altshuler DM, Durbin RM, Abecasis GR, Bentley DR, Chakravarti A, Clark
483 AG, Donnelly P, Eichler EE, Flicek P, Gabriel SB, Gibbs RA, Green ED, Hurler ME, Knoppers
484 BM, Korbel JO, Lander ES, Lee C, Lehrach H, Mardis ER, Marth GT, McVean GA, Nickerson
485 DA, Schmidt JP, Sherry ST, Wang J, Wilson RK, Gibbs RA, Boerwinkle E, Doddapaneni H, Han
486 Y, Korchina V, Kovar C, Lee S, Muzny D, Reid JG, Zhu Y, Wang J, Chang Y, Feng Q, Fang X,
487 Guo X, Jian M, Jiang H, Jin X, Lan T, Li G, Li J, Li Y, Liu S, Liu X, Lu Y, Ma X, Tang M, Wang
488 B, Wang G, Wu H, Wu R, Xu X, Yin Y, Zhang D, Zhang W, Zhao J, Zhao M, Zheng X, Lander
489 ES, Altshuler DM, Gabriel SB, Gupta N, Gharani N, Toji LH, Gerry NP, Resch AM, Flicek P,
490 Barker J, Clarke L, Gil L, Hunt SE, Kelman G, Kulesha E, Leinonen R, McLaren WM,
491 Radhakrishnan R, Roa A, Smirnov D, Smith RE, Stretter I, Thormann A, Toneva I, Vaughan B,
492 Zheng-Bradley X, Bentley DR, Grocock R, Humphray S, James T, Kingsbury Z, Lehrach H,
493 Sudbrak R, Albrecht MW, Amstislavskiy VS, Borodina TA, Lienhard M, Mertes F, Sultan M,
494 Timmermann B, Yaspo M-L, Mardis ER, Wilson RK, Fulton L, Fulton R, Sherry ST, Ananiev V,
495 Belaia Z, Beloslyudtsev D, Bouk N, Chen C, Church D, Cohen R, Cook C, Garner J, Hefferon T,
496 Kimelman M, Liu C, Lopez J, Meric P, O’Sullivan C, Ostapchuk Y, Phan L, Ponomarov S,
497 Schneider V, Shekhtman E, Sirotkin K, Slotta D, Zhang H, McVean GA, Durbin RM,
498 Balasubramaniam S, Burton J, Danecek P, Keane TM, Kolb-Kokocinski A, McCarthy S, Stalker J,
499 Quail M, Schmidt JP, Davies CJ, Gollub J, Webster T, Wong B, Zhan Y, Auton A, Campbell CL,
500 Kong Y, Marcketta A, Gibbs RA, Yu F, Antunes L, Bainbridge M, Muzny D, Sabo A, Huang Z,
501 Wang J, Coin LJM, Fang L, Guo X, Jin X, Li G, Li Q, Li Y, Li Z, Lin H, Liu B, Luo R, Shao H,
502 Xie Y, Ye C, Yu C, Zhang F, Zheng H, Zhu H, Alkan C, Dal E, Kahveci F, Marth GT, Garrison
503 EP, Kural D, Lee W-P, Fung Leong W, Stromberg M, Ward AN, Wu J, Zhang M, Daly MJ,
504 DePristo MA, Handsaker RE, Altshuler DM, Banks E, Bhatia G, del Angel G, Gabriel SB,
505 Genovese G, Gupta N, Li H, Kashin S, Lander ES, McCarroll SA, Nemesh JC, Poplin RE, Yoon
506 SC, Lihm J, Makarov V, Clark AG, Gottipati S, Keinan A, Rodriguez-Flores JL, Korbel JO,
507 Rausch T, Fritz MH, Stütz AM, Flicek P, Beal K, Clarke L, Datta A, Herrero J, McLaren WM,
508 Ritchie GRS, Smith RE, Zerbino D, Zheng-Bradley X, Sabeti PC, Shlyakhter I, Schaffner SF, Vitti
509 J, Cooper DN, Ball E V, Stenson PD, Bentley DR, Barnes B, Bauer M, Keira Cheetham R, Cox A,
510 Eberle M, Humphray S, Kahn S, Murray L, Peden J, Shaw R, Kenny EE, Batzer MA, Konkel MK,
511 Walker JA, MacArthur DG, Lek M, Sudbrak R, Amstislavskiy VS, Herwig R, Mardis ER, Ding L,
512 Koboldt DC, Larson D, Ye K, Gravel S, Consortium T 1000 GP, authors C, committee S, group P,

- 513 Medicine BC of, BGI-Shenzhen, Harvard BI of MIT and, Research CI for M, European Molecular
514 Biology Laboratory EBI, Illumina, Genetics MPI for M, University MGI at W, Health USNI of,
515 Oxford U of, Institute WTS, group A, Affymetrix, Medicine AEC of, University B, College B,
516 Laboratory CSH, University C, Laboratory EMB, University H, Database HGM, Sinai IS of M at
517 M, University LS, Hospital MG, University M, National Eye Institute NIH. 2015. A global
518 reference for human genetic variation. *Nature* **526**:68–74.
- 519 Babak T, DeVeale B, Tsang EK, Zhou Y, Li X, Smith KS, Kukurba KR, Zhang R, Li JB, van der Kooy
520 D. 2015. Genetic conflict reflected in tissue-specific maps of genomic imprinting in human and
521 mouse. *Nat Genet* **47**:544–549.
- 522 Ball MP, Li JB, Gao Y, Lee J-H, LeProust EM, Park I-H, Xie B, Daley GQ, Church GM. 2009.
523 Targeted and genome-scale strategies reveal gene-body methylation signatures in human cells. *Nat*
524 *Biotechnol* **27**:361–368.
- 525 Baran Y, Subramaniam M, Biton A, Tukiainen T, Tsang EK, Rivas MA, Pirinen M, Gutierrez-Arcelus
526 M, Smith KS, Kukurba KR. 2015. The landscape of genomic imprinting across diverse adult
527 human tissues. *Genome Res* **25**:927–936.
- 528 Bartolomei MS, Ferguson-Smith AC. 2011. Mammalian Genomic Imprinting. *Cold Spring Harb*
529 *Perspect Biol* **3**.
- 530 Bernstein BE, Stamatoyannopoulos JA, Costello JF, Ren B, Milosavljevic A, Meissner A, Kellis M,
531 Marra MA, Beaudet AL, Ecker JR, Farnham PJ, Hirst M, Lander ES, Mikkelsen TS, Thomson JA.
532 2010. The NIH Roadmap Epigenomics Mapping Consortium. *Nat Biotechnol* **28**:1045–1048.
- 533 Camargo M, Rivera D, Moreno L, Lidral AC, Harper U, Jones M, Solomon BD, Roessler E, Vélez JI,
534 Martínez AF, Chandrasekharappa SC, Arcos-Burgos M. 2012. GWAS reveals new recessive loci
535 associated with non-syndromic facial clefting. *Eur J Med Genet* **55**:510–514.
- 536 Chen Z, Zhang Y. 2020. Maternal H3K27me3-dependent autosomal and X chromosome imprinting. *Nat*
537 *Rev Genet* **21**:555–571.
- 538 Cheong CY, Chng K, Ng S, Chew SB, Chan L, Ferguson-Smith AC. 2015. Germline and somatic
539 imprinting in the nonhuman primate highlights species differences in oocyte methylation. *Genome*
540 *Res* **25**:611–623.
- 541 Chess A. 2013. Random and non-random monoallelic expression. *Neuropsychopharmacology* **38**:55–61.
- 542 Chiesa N, De Crescenzo A, Mishra K, Perone L, Carella M, Palumbo O, Mussa A, Sparago A, Cerrato
543 F, Russo S, Lapi E, Cubellis MV, Kanduri C, Cirillo Silengo M, Riccio A, Ferrero GB. 2012. The
544 KCNQ1OT1 imprinting control region and non-coding RNA: new properties derived from the
545 study of Beckwith-Wiedemann syndrome and Silver-Russell syndrome cases. *Hum Mol Genet*
546 **21**:10–25.
- 547 Court F, Tayama C, Romanelli V, Martin-Trujillo A, Iglesias-Platas I, Okamura K, Sugahara N, Simón
548 C, Moore H, Harness J V., Keirstead H, Sanchez-Mut JV, Kaneki E, Lapunzina P, Soejima H,
549 Wake N, Esteller M, Ogata T, Hata K, Nakabayashi K, Monk D. 2014. Genome-wide parent-of-
550 origin DNA methylation analysis reveals the intricacies of human imprinting and suggests a
551 germline methylation-independent mechanism of establishment. *Genome Res* **24**:554–569.
- 552 da Rocha ST, Gendrel A-V. 2019. The influence of DNA methylation on monoallelic expression. *Essays*
553 *Biochem* **63**:663–676.

- 554 Dahlet T, Argüeso Lleida A, Al Adhami H, Dumas M, Bender A, Ngondo RP, Tanguy M, Vallet J,
555 Auclair G, Bardet AF, Weber M. 2020. Genome-wide analysis in the mouse embryo reveals the
556 importance of DNA methylation for transcription integrity. *Nat Commun* **11**:3153.
- 557 De Coster W, De Rijk P, De Roeck A, De Pooter T, D’Hert S, Strazisar M, Slegers K, Van
558 Broeckhoven C. 2019. Structural variants identified by Oxford Nanopore PromethION sequencing
559 of the human genome. *Genome Res* **29**:1178–1187.
- 560 Gao F, Niu Y, Sun YE, Lu H, Chen Y, Li S, Kang Y, Luo Y, Si C, Yu J, Li C, Sun N, Si W, Wang H, Ji
561 W, Tan T. 2017. De novo DNA methylation during monkey pre-implantation embryogenesis. *Cell*
562 *Res* **27**:526–539.
- 563 Geneimprint. 2021. <http://www.geneimprint.com>
- 564 Gigante S, Gouil Q, Lucattini A, Keniry A, Beck T, Tinning M, Gordon L, Woodruff C, Speed TP,
565 Blewitt ME, Ritchie ME. 2019. Using long-read sequencing to detect imprinted DNA methylation.
566 *Nucleic Acids Res* **47**:e46–e46.
- 567 Goovaerts T, Steyaert S, Vandenbussche CA, Galle J, Thas O, Van Criekinge W, De Meyer T. 2018. A
568 comprehensive overview of genomic imprinting in breast and its deregulation in cancer. *Nat*
569 *Commun* **9**:1–14.
- 570 Hanna CW, Kelsey G. 2014. The specification of imprints in mammals. *Heredity (Edinb)* **113**:176–183.
- 571 Hashimoto H, Wang D, Horton JR, Zhang X, Corces VG, Cheng X. 2017. Structural Basis for the
572 Versatile and Methylation-Dependent Binding of CTCF to DNA. *Mol Cell* **66**:711–720.e3.
- 573 Hernandez Mora JR, Tayama C, Sánchez-Delgado M, Monteagudo-Sánchez A, Hata K, Ogata T,
574 Medrano J, Poo-Llanillo ME, Simón C, Moran S, Esteller M, Tenorio J, Lapunzina P, Kagami M,
575 Monk D, Nakabayashi K. 2018. Characterization of parent-of-origin methylation using the Illumina
576 Infinium MethylationEPIC array platform. *Epigenomics* **10**:941–954.
- 577 Hon GC, Rajagopal N, Shen Y, McCleary DF, Yue F, Dang MD, Ren B. 2013. Epigenetic memory at
578 embryonic enhancers identified in DNA methylation maps from adult mouse tissues. *Nat Genet*
579 **45**:1198–1206.
- 580 Jadhav B, Monajemi R, Gagalova KK, Ho D, Draisma HHM, van de Wiel MA, Franke L, Heijmans BT,
581 van Meurs J, Jansen R, Consortium G, Consortium B, ’t Hoen PAC, Sharp AJ, Kiełbasa SM. 2019.
582 RNA-Seq in 296 phased trios provides a high-resolution map of genomic imprinting. *BMC Biol*
583 **17**:50.
- 584 Jelinic P, Shaw P. 2007. Loss of imprinting and cancer. *J Pathol* **211**:261–268.
- 585 John RM, Lefebvre L. 2011. Developmental regulation of somatic imprints. *Differentiation* **81**:270–280.
- 586 Joshi RS, Garg P, Zaitlen N, Lappalainen T, Watson CT, Azam N, Ho D, Li X, Antonarakis SE,
587 Brunner HG, Buiting K, Cheung SW, Coffee B, Eggermann T, Francis D, Geraedts JP, Gimelli G,
588 Jacobson SG, Le Caignec C, de Leeuw N, Liehr T, Mackay DJ, Montgomery SB, Pagnamenta AT,
589 Papenhausen P, Robinson DO, Ruivenkamp C, Schwartz C, Steiner B, Stevenson DA, Surti U,
590 Wassink T, Sharp AJ. 2016. DNA Methylation Profiling of Uniparental Disomy Subjects Provides
591 a Map of Parental Epigenetic Bias in the Human Genome. *Am J Hum Genet* **99**:555–566.
- 592 Jung YH, Sauria MEG, Lyu X, Cheema MS, Ausio J, Taylor J, Corces VG. 2017. Chromatin States in
593 Mouse Sperm Correlate with Embryonic and Adult Regulatory Landscapes. *Cell Rep* **18**:1366–

- 594 1382.
- 595 Kent WJ, Sugnet CW, Furey TS, Roskin KM, Pringle TH, Zahler AM, Haussler D. 2002. The Human
596 Genome Browser at UCSC. *Genome Res* **12**:996–1006.
- 597 Khamlichi AA, Feil R. 2018. Parallels between mammalian mechanisms of monoallelic gene
598 expression. *Trends Genet* **34**:954–971.
- 599 Kim S, Scheffler K, Halpern AL, Bekritsky MA, Noh E, Källberg M, Chen X, Kim Y, Beyter D,
600 Krusche P, Saunders CT. 2018. Strelka2: fast and accurate calling of germline and somatic variants.
601 *Nat Methods* **15**:591–594.
- 602 Laurent L, Wong E, Li G, Huynh T, Tsirigos A, Ong CT, Low HM, Kin Sung KW, Rigoutsos I, Loring
603 J, Wei C-L. 2010. Dynamic changes in the human methylome during differentiation. *Genome Res*
604 **20**:320–331.
- 605 Li H. 2018. Minimap2: pairwise alignment for nucleotide sequences. *Bioinformatics* **34**:3094–3100.
- 606 Li H, Durbin R. 2009. Fast and accurate short read alignment with Burrows–Wheeler transform.
607 *Bioinformatics* **25**:1754–1760.
- 608 Matsubara K, Itoh M, Shimizu K, Saito S, Enomoto K, Nakabayashi K, Hata K, Kurosawa K, Ogata T,
609 Fukami M, Kagami M. 2019. Exploring the unique function of imprinting control centers in the
610 PWS/AS-responsible region: finding from array-based methylation analysis in cases with variously
611 sized microdeletions. *Clin Epigenetics* **11**:36.
- 612 Maupetit-Méhouas S, Montibus B, Nury D, Tayama C, Wassef M, Kota SK, Fogli A, Cerqueira Campos
613 F, Hata K, Feil R, Margueron R, Nakabayashi K, Court F, Arnaud P. 2016. Imprinting control
614 regions (ICRs) are marked by mono-allelic bivalent chromatin when transcriptionally inactive.
615 *Nucleic Acids Res* **44**:621–635.
- 616 Moore LD, Le T, Fan G. 2013. DNA Methylation and Its Basic Function. *Neuropsychopharmacology*
617 **38**:23–38.
- 618 Morison IM, Paton CJ, Cleverley SD. 2001. The imprinted gene and parent-of-origin effect database.
619 *Nucleic Acids Res* **29**:275–276.
- 620 Okae H, Chiba H, Hiura H, Hamada H, Sato A, Utsunomiya T, Kikuchi H, Yoshida H, Tanaka A,
621 Suyama M, Arima T. 2014. Genome-wide analysis of DNA methylation dynamics during early
622 human development. *PLoS Genet* **10**:e1004868–e1004868.
- 623 Puerta MF, Ruth C, Fang L, Robert P, Zhong D, A. R-MY, S. BM, M. LP, Qiyi T, L. H-F. 2014. CTCF
624 Binding to the First Intron of the Major Immediate Early (MIE) Gene of Human Cytomegalovirus
625 (HCMV) Negatively Regulates MIE Gene Expression and HCMV Replication. *J Virol* **88**:7389–
626 7401.
- 627 Renda M, Baglivo I, Burgess-Beusse B, Esposito S, Fattorusso R, Felsenfeld G, Pedone P V. 2007.
628 Critical DNA Binding Interactions of the Insulator Protein CTCF: A SMALL NUMBER OF ZINC
629 FINGERS MEDIATE STRONG BINDING, AND A SINGLE FINGER-DNA INTERACTION
630 CONTROLS BINDING AT IMPRINTED LOCI *. *J Biol Chem* **282**:33336–33345.
- 631 Romanelli V, Nakabayashi K, Vizoso M, Moran S, Iglesias-Platas I, Sugahara N, Simón C, Hata K,
632 Esteller M, Court F, Monk D. 2014. Variable maternal methylation overlapping the
633 nc886/vtRNA2-1 locus is locked between hypermethylated repeats and is frequently altered in

- 634 cancer. *Epigenetics* **9**:783–790.
- 635 Saenz-de-Juano MD, Ivanova E, Billooye K, Herta A-C, Smitz J, Kelsey G, Anckaert E. 2019. Genome-
636 wide assessment of DNA methylation in mouse oocytes reveals effects associated with in vitro
637 growth, superovulation, and sexual maturity. *Clin Epigenetics* **11**:197.
- 638 Shafin K, Pesout T, Lorig-Roach R, Haukness M, Olsen HE, Bosworth C, Armstrong J, Tigyi K, Maurer
639 N, Koren S, Sedlazeck FJ, Marschall T, Mayes S, Costa V, Zook JM, Liu KJ, Kilburn D, Sorensen
640 M, Munson KM, Vollger MR, Monlong J, Garrison E, Eichler EE, Salama S, Haussler D, Green
641 RE, Akeson M, Phillippy A, Miga KH, Carnevali P, Jain M, Paten B. 2020. Nanopore sequencing
642 and the Shasta toolkit enable efficient de novo assembly of eleven human genomes. *Nat Biotechnol*.
- 643 Sharp AJ, Migliavacca E, Dupre Y, Stathaki E, Sailani MR, Baumer A, Schinzel A, Mackay DJ,
644 Robinson DO, Cobellis G, Cobellis L, Brunner HG, Steiner B, Antonarakis SE. 2010. Methylation
645 profiling in individuals with uniparental disomy identifies novel differentially methylated regions
646 on chromosome 15. *Genome Res* **20**:1271–1278.
- 647 Silver MJ, Kessler NJ, Hennig BJ, Dominguez-Salas P, Laritsky E, Baker MS, Coarfa C, Hernandez-
648 Vargas H, Castelino JM, Routledge MN, Gong YY, Herczeg Z, Lee YS, Lee K, Moore SE, Fulford
649 AJ, Prentice AM, Waterland RA. 2015. Independent genomewide screens identify the tumor
650 suppressor VTRNA2-1 as a human epiallele responsive to periconceptional environment. *Genome*
651 *Biol* **16**:118.
- 652 Simpson JT, Workman RE, Zuzarte PC, David M, Dursi LJ, Timp W. 2017. Detecting DNA cytosine
653 methylation using nanopore sequencing. *Nat Methods* **14**:407.
- 654 Smith ZD, Meissner A. 2013. DNA methylation: roles in mammalian development. *Nat Rev Genet*
655 **14**:204–220.
- 656 Steijger T, Abril JF, Engström PG, Kokocinski F, Hubbard TJ, Guigó R, Harrow J, Bertone P. 2013.
657 Assessment of transcript reconstruction methods for RNA-seq. *Nat Methods* **10**:1177–1184.
- 658 Tomizawa S, Sasaki H. 2012. Genomic imprinting and its relevance to congenital disease, infertility,
659 molar pregnancy and induced pluripotent stem cell. *J Hum Genet* **57**:84–91.
- 660 Tung J, Barreiro LB, Johnson ZP, Hansen KD, Michopoulos V, Toufexis D, Michelini K, Wilson ME,
661 Gilad Y. 2012. Social environment is associated with gene regulatory variation in the rhesus
662 macaque immune system. *Proc Natl Acad Sci U S A* **109**:6490–6495.
- 663 Turan S, Bastepe M. 2013. The GNAS complex locus and human diseases associated with loss-of-
664 function mutations or epimutations within this imprinted gene. *Horm Res Paediatr* **80**:229–241.
- 665 Virtanen P, Gommers R, Oliphant TE, Haberland M, Reddy T, Cournapeau D, Burovski E, Peterson P,
666 Weckesser W, Bright J, van der Walt SJ, Brett M, Wilson J, Millman KJ, Mayorov N, Nelson ARJ,
667 Jones E, Kern R, Larson E, Carey CJ, Polat İ, Feng Y, Moore EW, VanderPlas J, Laxalde D,
668 Perktold J, Cimrman R, Henriksen I, Quintero EA, Harris CR, Archibald AM, Ribeiro AH,
669 Pedregosa F, van Mulbregt P, Vijaykumar A, Bardelli A Pietro, Rothberg A, Hilboll A, Kloeckner
670 A, Scopatz A, Lee A, Rokem A, Woods CN, Fulton C, Masson C, Häggström C, Fitzgerald C,
671 Nicholson DA, Hagen DR, Pasechnik D V, Olivetti E, Martin E, Wieser E, Silva F, Lenders F,
672 Wilhelm F, Young G, Price GA, Ingold G-L, Allen GE, Lee GR, Audren H, Probst I, Dietrich JP,
673 Silterra J, Webber JT, Slavič J, Nothman J, Buchner J, Kulick J, Schönberger JL, de Miranda
674 Cardoso JV, Reimer J, Harrington J, Rodríguez JLC, Nunez-Iglesias J, Kuczynski J, Tritz K,
675 Thoma M, Newville M, Kümmerer M, Bolingbroke M, Tartre M, Pak M, Smith NJ, Nowaczyk N,

- 676 Shebanov N, Pavlyk O, Brodtkorb PA, Lee P, McGibbon RT, Feldbauer R, Lewis S, Tygier S,
677 Sievert S, Vigna S, Peterson S, More S, Pudlik T, Oshima T, Pingel TJ, Robitaille TP, Spura T,
678 Jones TR, Cera T, Leslie T, Zito T, Krauss T, Upadhyay U, Halchenko YO, Vázquez-Baeza Y,
679 Contributors S 1. . 2020. SciPy 1.0: fundamental algorithms for scientific computing in Python. *Nat*
680 *Methods* **17**:261–272.
- 681 Xie W, Barr CL, Kim A, Yue F, Lee AY, Eubanks J, Dempster EL, Ren B. 2012. Base-Resolution
682 Analyses of Sequence and Parent-of-Origin Dependent DNA Methylation in the Mouse Genome.
683 *Cell* **148**:816–831.
- 684 Yang X, Han H, De Carvalho DD, Lay FD, Jones PA, Liang G. 2014. Gene body methylation can alter
685 gene expression and is a therapeutic target in cancer. *Cancer Cell* **26**:577–590.
- 686 Zhao H, Sun Z, Wang J, Huang H, Kocher J-P, Wang L. 2014. CrossMap: a versatile tool for coordinate
687 conversion between genome assemblies. *Bioinformatics* **30**:1006–1007.
- 688 Zink F, Magnusdottir DN, Magnusson OT, Walker NJ, Morris TJ, Sigurdsson A, Halldorsson GH,
689 Gudjonsson SA, Melsted P, Ingimundardottir H, Kristmundsdottir S, Alexandersson KF,
690 Helgadóttir A, Gudmundsson J, Rafnar T, Jonsdóttir I, Holm H, Eyjólfsson GI, Sigurdardóttir O,
691 Ólafsson I, Masson G, Gudbjartsson DF, Thorsteinsdóttir U, Halldorsson B V, Stacey SN,
692 Stefansson K. 2018. Insights into imprinting from parent-of-origin phased methylomes and
693 transcriptomes. *Nat Genet* **50**:1542–1552.
- 694 Zook JM, Catoe D, McDaniel J, Vang L, Spies N, Sidow A, Weng Z, Liu Y, Mason CE, Alexander N,
695 Henaff E, McIntyre ABR, Chandramohan D, Chen F, Jaeger E, Moshrefi A, Pham K, Stedman W,
696 Liang T, Saghbini M, Dzakula Z, Hastie A, Cao H, Deikus G, Schadt E, Sebra R, Bashir A, Truty
697 RM, Chang CC, Gulbahce N, Zhao K, Ghosh S, Hyland F, Fu Y, Chaisson M, Xiao C, Trow J,
698 Sherry ST, Zaranek AW, Ball M, Bobe J, Estep P, Church GM, Marks P, Kyriazopoulou-
699 Panagiotopoulou S, Zheng GXY, Schnall-Levin M, Ordonez HS, Mudivarti PA, Giorda K, Sheng
700 Y, Rypdal KB, Salit M. 2016. Extensive sequencing of seven human genomes to characterize
701 benchmark reference materials. *Sci Data* **3**:160025.
- 702 Zook JM, McDaniel J, Olson ND, Wagner J, Parikh H, Heaton H, Irvine SA, Trigg L, Truty R, McLean
703 CY, De La Vega FM, Xiao C, Sherry S, Salit M. 2019. An open resource for accurately
704 benchmarking small variant and reference calls. *Nat Biotechnol* **37**:561–566.
- 705